Applied and Environmental Microbiology, Oct. 2008, p. 6306–6312 Vol. 74, No. 20
0099-2240/08/$08.00+0 doi:10.1128/AEM.00877-08

Metabolic Microenvironmental Control by Photosynthetic Biofilms under Changing Macroenvironmental Temperature and pH Conditions▽†

Andrew Bissett,[1]* Andreas Reimer,[2] Dirk de Beer,[1] Fumito Shiraishi,[2] and Gernot Arp[2]

Max Planck Institute for Marine Microbiology, Celsiusstraße 1, D-28359 Bremen, Germany,[1] and Geoscience Centre, University of Göttingen, Goldschmidtstraße 3, D-37077 Göttingen, Germany[2]

Received 17 April 2008/Accepted 1 August 2008

Ex situ microelectrode experiments, using cyanobacterial biofilms from karst water creeks, were conducted under various pH, temperature, and constant-alkalinity conditions to investigate the effects of changing environmental parameters on cyanobacterial photosynthesis-induced calcification. Microenvironmental chemical conditions around calcifying sites were controlled by metabolic activity over a wide range of photosynthesis and respiration rates, with little influence from overlying water conditions. Regardless of overlying water pH levels (from 7.8 to 8.9), pH at the biofilm surface was approximately 9.4 in the light and 7.8 in the dark. The same trend was observed at various temperatures (4°C and 17°C). Biological processes control the calcium carbonate saturation state (Ω) in these and similar systems and are able to maintain Ω at approximately constant levels over relatively wide environmental fluctuations. Temperature did, however, have an effect on calcification rate. Calcium flux in this system is limited by its diffusion coefficient, resulting in a higher calcium flux (calcification and dissolution) at higher temperatures, despite the constant, biologically mediated pH. The ability of biological systems to mitigate the effects of environmental perturbation is an important factor that must be considered when attempting to predict the effects of increased atmospheric partial CO_2 pressure on processes such as calcification and in interpreting microfossils in the fossil record.

Calcifying biofilms have contributed significantly to the formation of carbonate sediments throughout earth history (8, 24, 27). These sediments are known as microbialites and, if macroscopically laminated, stromatolites. Their temporal and geographic distributions have been used to infer the impacts of metazoan evolution (4, 33) and changes in ocean chemistry (2, 13, 26). Many stromatolites are formed in the photic zone of shallow-water environments by thin cyanobacterial biofilms, rather than by thick microbial mats, which tend to produce more irregular fabrics.

The principal mechanisms involved in stromatolite formation are (i) heterogeneous crystal nucleation at acidic extracellular polymeric substances (1, 19, 22, 32) and (ii) increases in the $Ca^{2+} \times CO_3^{2-}$ ion activity product (IAP), which may be induced by microbial activity (e.g., photosynthesis, sulfate reduction) and/or external physicochemical factors (e.g., evaporation, CO_2 degassing) (5, 21, 25, 31). Lamination of microbialite deposits may result from a number of factors, including seasonally induced changes to calcification processes caused by changes in biofilm composition and calcium carbonate mineral supersaturation. Some calcifying biofilms exhibit fabrics containing cyanobacterial $CaCO_3$ tubes which can be preserved as microfossils known as *Girvanella* or *Cayeuxia* (25, 34). These cyanobacterial tubes have been attributed to photosynthesis-induced pH microgradients under conditions of low dissolved-inorganic-carbon (DIC) levels and, consequently, low bulk-phase pH buffering (2). Specifically, the impact of a given amount of DIC removal on changes in $CaCO_3$ supersaturation should, theoretically, increase with decreasing DIC concentrations and initial pHs at a given IAP. Other factors that have been discussed in this context are temperature and $CaCO_3$ mineral supersaturation (14, 26).

Changing environmental conditions (e.g., temperature and pH) may affect biological activity and calcification. Precipitation and dissolution may be affected by warming-induced changes, as brought about by global climate change, and/or by changes to overlying water pH, brought about by changes to atmospheric partial CO_2 pressure (pCO_2), in rainfall patterns or trophic state. Understanding the effects of changing environmental conditions on calcification and dissolution processes is important, both to the prediction of the effects of global climate change and to the interpretation of the paleo record.

The influence of diurnal temperature changes on hydrochemistry in karst water creeks has been investigated previously (12), and from these changes, inferences regarding precipitation processes were made. Drysdale et al. (12) reported a strong diurnal pattern to hydrochemistry and calcite saturation in what they considered to be a karst system with solely inorganic precipitation. They reported that diurnal fluctuations in temperature significantly altered the creek's carbonate chemistry and led to changes in rates and reach of precipitation. Changing environmental factors such as temperature also influence biotic processes such as photosynthesis and respiration. In karst systems such as those investigated here, in which biofilms play a significant role in controlling the chemical conditions at the sites of mineral nucleation (6), fluctuations in abiotic conditions may also affect stromatolite formation pro-

* Corresponding author. Present address: CSIRO, Plant Industry, P. O. Box 1600, Canberra, ACT 2601, Australia. Phone: 61 (0)2 6246 4820. Fax: 61 (0)2 6246 5000. E-mail: Andrew.Bissett@csiro.au.

† Supplemental material for this article may be found at http://aem.asm.org/.

▽ Published ahead of print on 8 August 2008.

cesses. These effects may be manifested as changes to rates of precipitation/dissolution or as mitigating effects of the biofilm against bulk water changes.

Despite the importance of understanding these processes to both projections of biological response to climate change and to paleoenvironmental interpretations, experimental studies on calcification in cyanobacterial communities are rare (e.g. (11, 18), and the specific relationship between various environmental factors, such as temperature and pH conditions, on photosynthesis-induced calcification of cyanobacterial biofilms have not, thus far, been investigated. Temperature changes may alter the rate of abiotic degassing and the rate of biological processes and, hence, precipitation. Changes to bulk water pH will alter the bulk water $CaCO_3$ saturation state but may not have such a great effect at the stromatolite surface, if biological processes are maintained. In this study, the results of ex situ microelectrode experimental studies using cyanobacterial biofilms from karst water creeks under various bulk water conditions are presented and discussed with respect to their implications for prediction of climate-induced changes to calcification and to interpretation of the paleoenvironmental record.

MATERIALS AND METHODS

Samples and sample collection. Samples were collected from the Deinschwanger Bach, as described in reference 6. The Deinschwanger Bach is located near Nuremberg (49°23′N, 11°28′E) in southern Germany and has been used for previous studies on cyanobacterial biofilm calcification. It is described in more detail in reference 3 and shows active laminar stromatolite formation up to 1.8 mm/year.

Samples were collected from two distinct, active tufa-forming sites for pH manipulation experiments. Site 1 comprised a small stromatolite cascade 65 m downstream from a minor spring, which entered the creek's main flow approximately 40 m after the cascade. At this site, the water was approximately 1- to 5-cm deep and exhibited a fast flow rate (approximately 40 cm s^{-1}) and, consequently, a small diffusive boundary layer (DBL; approximately 200 to 300 μm). Stromatolite at site 1 was laminated and several centimeters thick. Site 2 was a well-illuminated section of the lower creek, approximately 20-cm deep, and had a slower flow rate (approximately 10 cm s^{-1}) than, but similar DBL (approximately 200 μm) to, site 1. Site 2 exhibited thin (up to 1 mm) fragile carbonate crusts. Samples from site 2 only were used for temperature manipulation experiments. Samples were removed from the creek with a motorized core-drilling device (modified Stihl chainsaw) and stored in ambient creek water in coolers until they were returned to the laboratory, within 24 h. Creek water samples for the experiments were collected without air bubbles in 20-liter plastic containers and stored at 4°C in the dark until use.

Laboratory setup. Once in the laboratory, samples were stored in temperature-controlled, aerated, recirculating aquariums (total volume, approximately 30 liters) containing creek water. Phototrophic community composition did not change during transport and incubation (6). Samples were removed to flow cells connected to the same recirculating water supply for measurements during experiments run at ambient temperature and experimentally altered temperatures. Experimental flow rates were approximately 0.03 liter s^{-1}. A reservoir of creek water separate from the main holding aquarium's supply was used for pH-manipulated experiments. pH was manipulated by the addition of CO_2, in bottled Vilsa (Germany) mineral water, to lower pH or by aerating the reservoir with CO_2-free air (air scrubbed in NaOH) to raise it. Vilsa water (http://www.pmgeiser.ch/mineral/index.php?func=dispes&parval=54) contains only trace mineral components. Amounts added to 30-liter experimental setups were <20 ml and were deemed to have had no effect on overall water chemistry. During pH adjustments, pH was monitored continuously with an MA130 ion detector (Mettler Toledo, Columbus, OH). Rates of CO_2 addition or removal were adjusted to maintain the desired pH.

Microelectrode measurements comprised three sets. The first consisted of measurements of O_2, pH, and Ca^{2+} concentration profiles on samples held at ambient creek conditions (temperature, 10°C; pH 8.4). The second comprised measurements of concentration gradients of the same ions in the sample at a pH raised to 8.9 and at a pH lowered to lowered 7.8. The final set of measurements, involving the same ions as those in the previous experiments, were on temperature-adjusted samples from the Deinschwanger Bach collected 12 months later. In this set of measurements, temperature was raised from the ambient 10°C to 17°C and lowered to 4°C.

Microelectrode measurements and calculations. Liquid membrane Ca^{2+} and pH sensors were prepared and calibrated as described previously (9, 10). Fast-responding O_2 microsensors were also prepared as described previously (23). All electrodes were placed manually at the stromatolite surface while viewing the sample through a dissection microscope. The stromatolite surface was then set at 0 cm. All measurements were made at measured distances above the stromatolite. Negative distances, therefore, indicate that the sensor is above the stromatolite/water interface. Profiling was automated after electrodes were positioned at the stromatolite surface. Sensors were connected to a micromanipulator, which was fixed to a motorized stage (VT-150; Micos, Eschbach, Germany) and allowed reproducible positioning of the sensor tip with 1-μm precision. The microelectrodes were connected to a picoammeter (O_2 electrode) or a millivoltmeter, and the meter output was collected by a data acquisition device (NI DaqPad-6015; National Instruments, Austin, TX). After positioning at the surface, profiling was performed automatically. Motor control and data acquisition were performed with a computer and custom-written software (μ-Profiler; provided by Lubos Polerecky). All profiles were corrected for offset to ion levels in the bulk liquid; oxygen concentrations in the bulk liquid were determined from literature values at experimental temperatures (salinity = 0 ppt), pH as described above, Ca^{2+} by inductively coupled plasma-optical emission spectroscopy (Perkin Elmer Optima 3300 DV) and DIC by CO_2 coulometer (UIC Coulometrics, Joliet, IL).

Interfacial fluxes (J) were calculated from the concentration profiles by using Fick's first law: $J = D \times (dc/dx)$, where D is the diffusion coefficient and dc/dx is the interfacial concentration gradient, i.e., the concentration gradient in the mass boundary layer directly adjacent to the stromatolite surface.

Calcite saturation is given by the saturation state omega (Ω): $\Omega = Ca^{2+} \times CO_3^{2-}/K_{calcite}$, where the numerator is the IAP and the denominator the solubility product $K_{calcite}$ as given by reference 20. Carbonate concentrations were determined from bulk water DIC and pH microprofiles. For the calculation of $\Omega_{calcite}$, activities were estimated by applying the activity coefficients of water used in experiments as delivered from the PHREEQC program (0.686 for Ca^{2+} and CO_3^{2-}).

Diffusion coefficients. The diffusion coefficients of O_2 and Ca^{2+} are literature-derived values corrected for temperature and type of counter ion (7, 16). Diffusion coefficients for oxygen that we used were as follows: at 4°C, 1.28×10^{-9} m^2 s^{-1}; at 10°C, 1.57×10^{-9} m^2 s^{-1}; and at 17°C, 1.934×10^{-9} m^2 s^{-1}. Diffusion coefficients that we used for Ca^{2+} with HCO_3^- as counter ion were as follows: at 4°C, 0.546×10^{-9} m^2 s^{-1}; at 10°C, 0.67×10^{-9} m^2 s^{-1}; and at 17°C, 0.827×10^{-9} m^2 s^{-1}.

Statistical analyses. Analysis of variance was used to test for the effects of treatment on chemical flux rates. Tests were conducted separately for each chemical flux (Ca^{2+}, O_2) and at each light phase (light or dark) for each pH and temperature treatment. Homogeneity of variances was checked visually by examining residual plots. Data that did not meet this assumption of analysis of variance were log transformed. Significant factors were compared using Tukey's honestly significant difference post hoc tests. All statistical tests were performed at an α of 0.05, with $F_{2,5}$, using the statistical software SPSS version 10.

RESULTS

Steady-state microsensor profiles were obtained for all treatments and displayed typical variation (see Fig. S1 in the supplemental material). The steady state was reached very quickly (<10 min) both after switching on and turning off the lights. Calcium fluxes have been shown previously to represent $CaCO_3$ dissolution and precipitation in these stromatolites (6, 29). Biofilms were able to control microenvironmental conditions under all experimental conditions. Changing overlying water pH and temperature had little effect on biofilm Ω state. Temperature did, however, affect calcium fluxes by influencing calcium ion diffusion coefficients.

pH manipulations. Concentration profiles of O_2, pH, and Ca^{2+} were measured on all samples (Fig. 1) at experimentally manipulated pHs. It should be noted that slight discrepancies

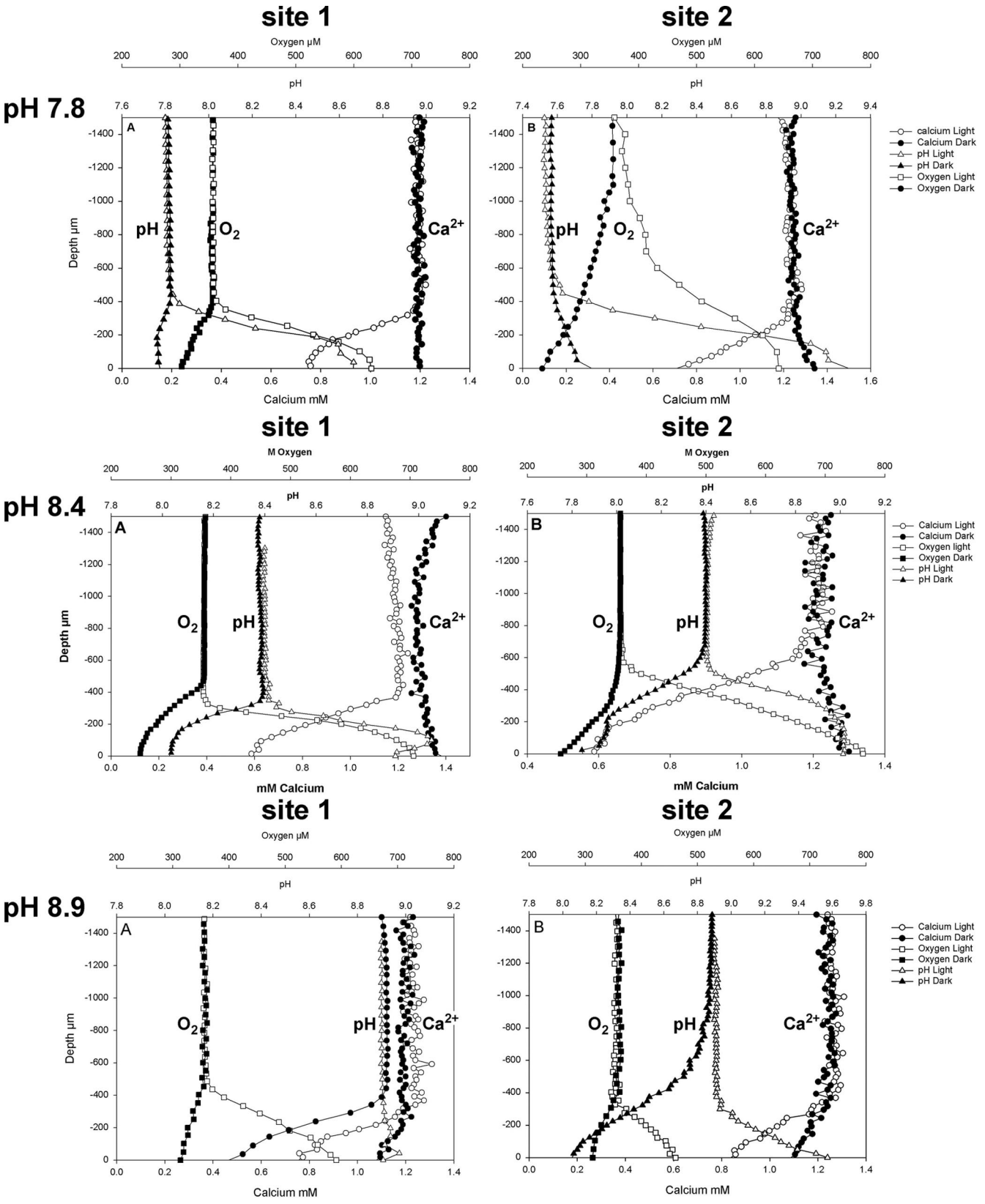

FIG. 1. pH, O_2, and Ca^{2+} profiles in the light and dark at the three experimental pHs for site 1 and site 2.

TABLE 1. Fluxes of oxygen and calcium (mean ± standard error; $n = 2$) and pH changes at biofilm surfaces measured in samples from the Deinschwanger Bach[a]

Site	pH		Flux (mol m^{-2} s^{-1})				ΔpH	
			O_2		Ca^{2+}			
	Experimental	Initial	Light	Dark	Light	Dark	Light	Dark
1	7.8	7.8	$1.7 \times 10^{-6} \pm 7.1 \times 10^{-8}$*	$-2.4 \times 10^{-7} \pm 2.3 \times 10^{-9}$*	$-1.2 \times 10^{-6} \pm 2.5 \times 10^{-8}$*	0*	0.86	−0.04
	8.4	8.4	$4.4 \times 10^{-6} \pm 1.4 \times 10^{-6}$*	$-3.8 \times 10^{-7} \pm 1.4 \times 10^{-7}$*	$-1.3 \times 10^{-6} \pm 1.5 \times 10^{-8}$*	$1.2 \times 10^{-7} \pm 1.3 \times 10^{-8}$**	0.54	−0.36
	8.9	8.9	$1.1 \times 10^{-6} \pm 2.1 \times 10^{-7}$*	$-1.4 \times 10^{-7} \pm 1.0 \times 10^{-8}$*	$-1.4 \times 10^{-6} \pm 8.5 \times 10^{-8}$*	$-5.1 \times 10^{-7} \pm 6.1 \times 10^{-8}$**	0.07	−0.66
2	7.8	7.6	$8.0 \times 10^{-7} \pm 1.3 \times 10^{-8}$*	$-1.5 \times 10^{-7} \pm 3.0 \times 10^{-8}$*	$-1.1 \times 10^{-6} \pm 6.0 \times 10^{-8}$*	$3.3 \times 10^{-7} \pm 7.1 \times 10^{-8}$*	1.75	0.2
	8.4	8.4	$1.6 \times 10^{-6} \pm 7.5 \times 10^{-8}$*	$-4.3 \times 10^{-7} \pm 9.1 \times 10^{-8}$*	$-8.9 \times 10^{-7} \pm 5.4 \times 10^{-8}$*	0*	0.62	−0.48
	8.9	8.9	$6.4 \times 10^{-7} \pm 8.5 \times 10^{-8}$*	$-2.4 \times 10^{-7} \pm 1.0 \times 10^{-8}$*	$-7.9 \times 10^{-7} \pm 4.6 \times 10^{-8}$**	$-1.7 \times 10^{-7} \pm 7.3 \times 10^{-8}$*	0.67	−0.85

[a] For fluxes, positive values indicate flux from the biofilm to the water column, and negative values indicate the opposite. Values with the same number of asterisks (within each chemical and light phase at each site) were not significantly different ($P > 0.05$).

in the observed height of the DBL and bulk water concentrations of chemical species measured are evident in the results presented. The profiles presented are averages of two positions on each sample, and these variations indicate both the heterogeneity within the samples and the difficulty in aligning the various sensors to exactly the same position on each sample. The profiles do, however, show consistent results.

In all samples, photosynthesis increased O_2 concentration at the stromatolite surface in the light, causing a concomitant increase in pH and a decrease in Ca^{2+} ion concentration. In the dark, respiration resulted in a decrease in O_2 concentration and often a small decrease in pH and increase in Ca^{2+} concentration. In the high-pH (8.9) treatment, however, a decrease in calcium ion concentration was seen in both light and dark incubations.

Flux rates of O_2 and Ca^{2+} and pH changes (ΔpH) observed are presented in Table 1. In all treatments, pHs approached the same values (9.2 to 9.5) in light incubations, although there were some small differences, largely between sites. The fact that similar maximum pH values were reached in all treatments leads to different ΔpH values. Higher ΔpH values occurred in the low-pH (7.8) treatment than in the high-pH (8.9) treatment in the light. In the dark, the opposite trend was observed because pHs were always around 7.8, regardless of the overlying water pH. The highest fluxes of O_2 from the biofilm were seen in the samples at ambient pH (8.4) at both sites (statistically significant only at site 2; $P < 0.05$), as were the highest O_2 fluxes to the biofilm surface during dark incubations, although these were not significantly different ($P > 0.05$).

Calcium fluxes were very similar under all treatments at both sites but did display some minor variations (Table 1). At site 1, the light flux was highest at pH 8.9 but was not significantly different from that at 8.4 or 7.8 ($P > 0.05$). In the dark, there was a significant difference between the fluxes ($P < 0.05$). The lowest absolute flux was seen at pH 7.8, while the flux at pH 8.9 was actually toward the biofilm, indicating precipitation. At site 2, a different pattern was seen. Dark fluxes were still much lower than light fluxes and, except in the high-pH (8.9) treatment, were all away from the biofilm surface. In the light, the highest flux ($P < 0.05$) was observed in the lowest-pH (7.8) treatment. The data clearly show a biologically controlled, diurnal pattern of calcium precipitation.

Calcite saturation state microprofiles (Fig. 2), calculated from bulk water DIC, pH, and Ca^{2+} microprofiles, demonstrate the degree to which $\Omega_{calcite}$ is controlled by the carbonate system. $\Omega_{calcite}$ profiles mirrored pH profiles and indicated that the water was supersaturated with respect to calcite under all experimental conditions. At both sites, illumination caused a photosynthetically induced increase in $\Omega_{calcite}$. In turn, a clear decrease in $\Omega_{calcite}$ was evident at both sites without illumination. Despite these metabolically induced changes in $\Omega_{calcite}$, no relationship existed between the rate of calcification (derived from Ca^{2+} fluxes) and the degree of supersaturation.

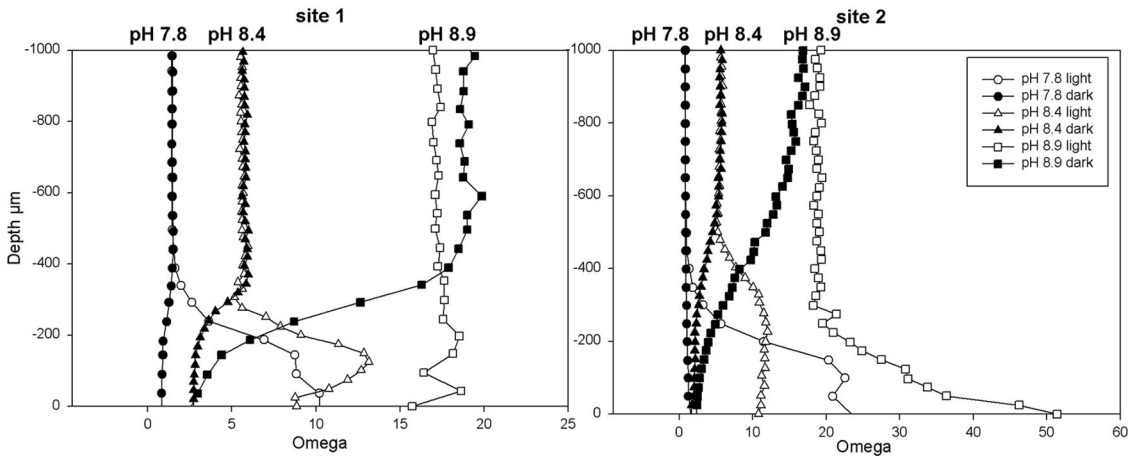

FIG. 2. Omega value profiles, calculated from Ca^{2+} profiles and alkalinity levels, for sites 1 and 2 at each experimental pH.

Temperature manipulations. The second experiment comprised manipulations of temperature, in order to investigate its effects on calcification. In light of the heterogeneity in each sample indicated by the pH experiment, concentration profiles in the temperature experiments were measured at the same location on each sample, and only samples from site 2 were used for the experiments. Temperatures tested were 4°C, 10°C (ambient), and 17°C. Measured profiles are presented in Fig. 3.

In all treatments, pHs approached the same values in both light and dark incubations, although there were some small differences (Table 2). The pH increased markedly under light conditions, from 8.4 to approximately 9.5 (maximum, 9.7). Under dark conditions, the pH decreased slightly, from 8.4 to approximately 8.1 at 10°C and 17°C, respectively, while no pH decrease was observed at 4°C.

Oxygen fluxes both away from and toward the sediment increased with the temperature in the light and dark, respectively (Table 2). Calcium flux was always toward the stromatolite biofilm surface under light conditions and increased with increasing temperature, although this increase was not statistically significant ($P > 0.05$). Dark fluxes were much lower than those seen under the light conditions, were always away from the stromatolite biofilm surface, and also increased with increasing temperature. Under dark conditions, no calcium flux was observed from or toward the stromatolite surface at 4°C (Table 2). Fluxes at 10°C and 17°C were significantly different from this.

DISCUSSION

The investigated biofilm community, rich in filamentous cyanobacteria, flourishes in its natural setting (hard-water creeks) under a wide range of pH and temperature conditions; the pH ranges from 7.6 (a short distance downstream from the spring) to 8.5 (lower creek sections and end of the carbonate deposition zone), with maximum values up to 9.3 measured within the biofilm microenvironment (6). The biofilm composition is described in detail by Shiraishi et al. (29). Phototrophic members of the biofilm were dominated by filamentous cyanobacteria (3- to 5-μm wide) of morphotype "*Phormidium incrustatum*" but also included *Lyngbya*-type and coccoid cyanobacteria and filamentous green algae of the genus *Cladophora*. Diatoms, such as *Achnanthes*, *Gomphonema*, *Nitzschia*, and *Navicula*, occurred in the upper biofilm. Nonphototrophic community members included heterotrophic bacteria, including sulfate-reducing bacteria and flavobacterial species. The cyanobacterial community composition was reasonably constant over the investigated zone, with only the immediate spring environment (pH 7.3 to 7.4) exhibiting distinct communities (unpublished data). In situ temperatures vary seasonally between 5°C and 13°C.

Experimental manipulations of pH and temperature conditions were conducted under conditions of constant alkalinity (3.0 mmol kg^{-1}) but various DIC (2.8 to 3.1 mmol kg^{-1}); pH conditions were manipulated by the addition of CO_2. Experimental flow rates were lower than in situ, resulting in slightly higher DBLs. We have shown previously (6) that photosynthesis increases when the DBL approaches 600 μm but that the in situ flow conditions used maintained a DBL of 400 μm or less

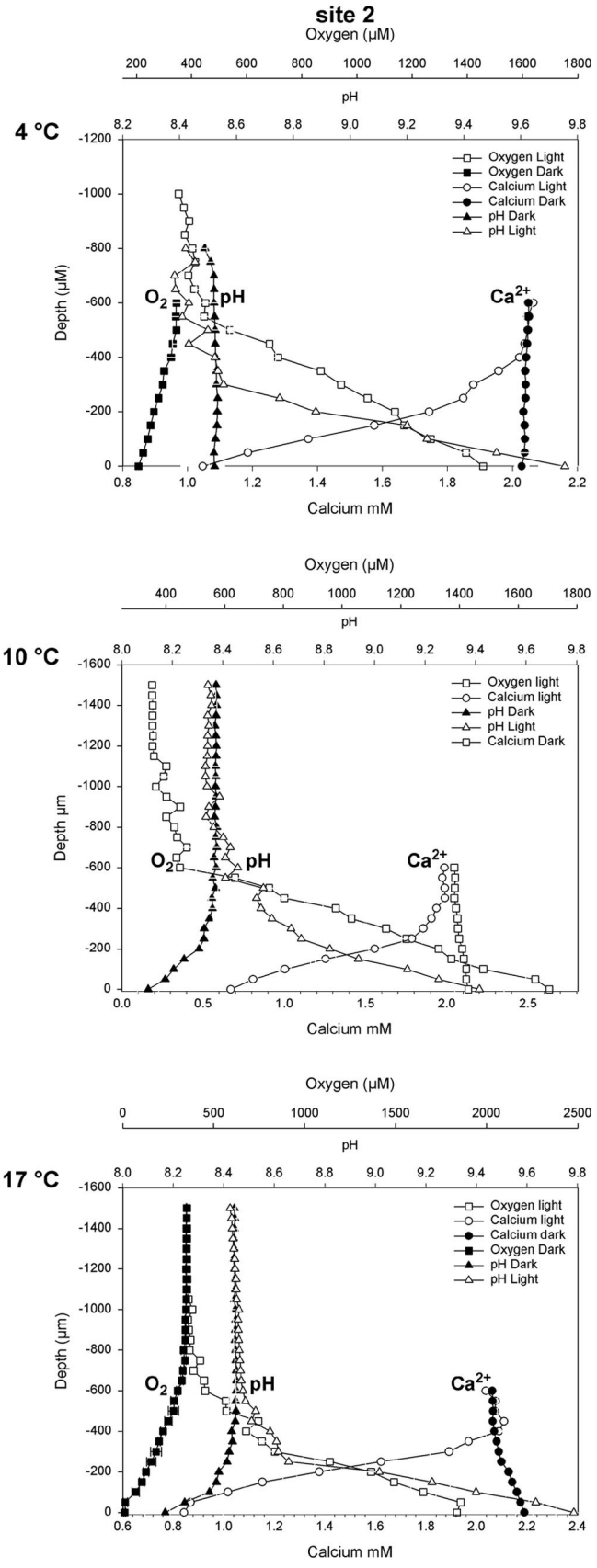

FIG. 3. pH, O_2, and Ca^{2+} profiles at each experimental temperature.

TABLE 2. Fluxes of oxygen and calcium (mean ± standard error; $n = 2$) and pH changes at biofilm surfaces measured in samples from Deinschwanger Bach at different temperatures[a]

Experimental temp	Flux (mol m^{-2} s^{-1})				ΔpH	
	O_2		Ca^{2+}		Light	Dark
	Light	Dark	Light	Dark		
4°C	$2.8 \times 10^{-6} \pm 1.6 \times 10^{-7}$*	$-3.7 \times 10^{-7} \pm 6.6 \times 10^{-8}$*	$-2.0 \times 10^{-6} \pm 2.4 \times 10^{-7}$*	0*	1.3	0
10°C	$3.0 \times 10^{-6} \pm 6.2 \times 10^{-7}$*	NA	$-3.5 \times 10^{-6} \pm 1.3 \times 10^{-6}$*	$2.0 \times 10^{-7} \pm 6.7 \times 10^{-8}$**	1.0	−0.3
17°C	$1.0 \times 10^{-5} \pm 8.7 \times 10^{-7}$**	$-1.0 \times 10^{-6} \pm 2.5 \times 10^{-8}$**	$-4.1 \times 10^{-6} \pm 3.9 \times 10^{-7}$*	$2.9 \times 10^{-7} \pm 5.0 \times 10^{-10}$**	1.3	−0.3

[a] For fluxes, positive values indicate flux from the biofilm to the water column, and negative values indicate the opposite. NA indicates that no profile was obtained. Values with the same number of asterisks (within each chemical and light phase) were not significantly different ($P > 0.05$).

and agreed well with in situ microsensor measurements, both in the dark and in the light.

Under illumination, photosynthesis consistently caused the pH at the biofilm surface to increase to approximately 9.4, regardless of overlying water pCO_2 (2,200 to 150 ppm V).

Changes similar to those with respect to the pH were noted for temperatures, except at 4°C, where biological activity was reduced to such an extent that changes were negligible. This difference in the ΔpH values in the light was observed despite the similar O_2 production rates. In the dark, the opposite was seen, i.e., respiration caused the pH to drop to approximately 7.8 regardless of pCO_2 or temperature. Again, this occurred despite similar O_2 consumption rates in the pH manipulation experiments. O_2 consumption rates were, however, lower at lower temperatures. The direction of the ΔpH value changes was as expected, i.e., photosynthesis increased pH, while in the dark, respiration led to its decrease. The differences in the magnitudes of ΔpH, resulting from different initial pH values but very similar final pH values, were unexpected. Several explanations for this phenomenon may be offered.

The first is that the observed ΔpH values were related to the physiological optima of the mat community. If this had been the case, the highest ΔpH value should have correlated with the highest O_2 fluxes, but this was not observed. O_2 fluxes at all pH treatments were reasonably similar, with the maximum flux actually occurring at a pH of 8.4, which is the pH of the creek section from which the samples were taken.

The second explanation for the ΔpH values observed is the possibility of different pH buffering capacities at the various initial pHs. In this model, the lowest ΔpH values should correlate with the highest buffering at $pK_a = 6.34$ and $pK_b = 10.36$. Our results, however, show that +ΔpH and −ΔpH have opposite trends for increasing bulk water pH values (Fig. 1). Furthermore, within the experimental pH range (7.8 to 8.9), which is near the half-equivalence point of 8.1, changes in pH buffering are very minor.

Third, the availability of DIC for photosynthesis may limit the extent of light-induced pH increases. As CO_2 is removed by photosynthesis and pH increases, less CO_2 is available. In the current system (alkalinity, 3 mmol kg^{-1}) at pH 7.8, approximately 4% (138 mmol m^{-3}) of DIC exists as CO_2, while at pH 8.9, this value is reduced to 0.3% (10 mmol m^{-3}). Several studies have shown that DIC may limit photosynthesis, and it was suggested by Larkum et al. (15) that when the pH exceeds the level at which DIC exists as CO_2, DIC must be consumed as HCO_3^-. In the biofilms investigated here, the pH never exceeds this level, although CO_2 does drop to a very low value (approximately 1 mmol m^{-3} at pH 9.5). Cyanobacteria may overcome CO_2 limitation via carbon-concentrating mechanisms, which effectively uncouple photosynthesis from CO_2 concentration. While these may have an effect on DIC chemistry at a cellular level, their effect on community level chemistry will be minimal. In essence, carbon-concentrating mechanisms do not change the stoichiometry of the processes and, thus, the local effects on pH. The fact that O_2 concentrations (the product of photosynthesis) remain well below overlying water DIC concentrations suggests that DIC is not limiting in this system. Even if DIC supply were limiting photosynthesis, the nature of +ΔpH and −ΔpH trends observed here would not be explained. There may indeed be some physiological limitation to the extent of physiologically induced +ΔpH value changes, but these should also be reflected in the O_2 production rates, which remain similar under all treatments. It is also possible that the calcification process limits the extent of pH changes and supports photosynthesis (17). For this to explain the observed ΔpH and O_2 production trends, we should see calcification rates increase with increasing pH. This is not the case. The explanation of DIC limitations also does not explain the observed −ΔpH value changes.

The final explanation for the observed results is a contribution from other unassessed processes (e.g., nitrate/ammonia assimilation), which may affect pH levels (30). The most probable explanation is some combination of all of the above, and further modeling and experimental work is required to address these issues.

Temperature manipulations were all conducted at pH 8.4, which was the in situ pH at the time of sampling. Temperature was clearly shown to affect biological activity, with O_2 fluxes increasing with increasing temperatures, both in the light and in the dark. Ca^{2+} fluxes (indicating, in this system, calcium carbonate precipitation and dissolution) (6) also increased with increasing temperatures (Table 2 and Fig. 3). Although these increases were not statistically significant in the experiments conducted, this may be explained by the small degrees of freedom used. The flux differences may be biologically important, and given that little change was observed in the biofilm surface pH and Ω values under all experimental conditions, it appears that the effects of temperature changes on the diffusion coefficients of Ca^{2+} and HCO_3^{2-} are important in determining flux rates. The diffusion coefficients increase with temperatures and, in these experiments, explain the magnitudes of increasing Ca^{2+} flux rates we observed.

Temperature, therefore, affects the possible transport limitations of precipitating chemicals, which in turn affects possible

rates of calcite deposition and dissolution. Although temperature increase leads to an increase in biological activity, ion diffusion velocity, and calcification in the light, the concomitant increase in dark parameters also increases dissolution, thereby maintaining similar net diel precipitation rates at all temperatures. For the interpretation of the fossil record of calcifying cyanobacteria, this implies that the abundance of cyanobacterial microfossils and related stromatolites appears not to be significantly affected by marine surface temperature variations, contrary to previous suggestions (21). This is true at least for the investigated range between 4°C and 17°C.

The ability of biological systems to control their microenvironment, and therefore create an environment very different from that of their wider surroundings, also leads to interesting implications for both the prediction of the effects of increasing atmospheric pCO_2 and the paleogeological interpretation of calcified microfossils. It appears that under high pCO_2 conditions, cyanobacterial calcification may be maintained by high CO_2 availability and proceed at low "apparent" pH (i.e., low pH in the overlying water). Therefore, as long as calcite saturation at the cell/biofilm surface remains >1, the formation of calcareous, tubular microfossils may still occur at low overlying water pH conditions (certainly between 7.8 to 8.4, as investigated here). Indeed the magnitude of Ω does not appear to influence the rate of calcification, but rather, once some Ω threshold (approximately 10) is reached, calcification may proceed. This is contradictory to the idea that increasing pCO_2 should reduce the potential of photosynthesis-induced calcification in cyanobacterial biofilms by lowering bulk phase pH and hence $CaCO_3$ mineral supersaturation (14, 28).

ACKNOWLEDGMENTS

We thank the microsensor technicians at the MPI, Bremen, Germany, for assistance with microsensor construction and Lubos Polerecky for the microprofiling software. We thank Hakhyun Nam (Kwangwoon University, South Korea) for supplying the carbonate ionophore.

This project is part of the Research Unit "Geobiology of organo- and biofilms," funded by the German Research Foundation (DFG-FOR 571, publication no. 23).

REFERENCES

1. **Aloisi, G., A. Gloter, M. Krüger, K. Wallmann, F. Guyot, and P. Zuddas.** 2006. Nucleation of calcium carbonate on bacterial nanoglobules. Geology **34:**1017–1020.
2. **Arp, G., A. Reimer, and J. Reitner.** 2001. Photosynthesis-induced biofilm calcification and calcium concentrations in phanerozoic oceans. Science **292:** 1701–1704.
3. **Arp, G., N. Wedemeyer, and J. Reitner.** 2001. Fluvial tufa formation in a hard-water creek (Deinschwanger Bach, Franconian Alb, Germany). Facies **44:**1–22.
4. **Awramik, S. M.** 1971. Precambrian columnar stromatolite diversity: reflection of metazoan appearance. Science **174:**825–827.
5. **Baumgartner, L. K., R. P. Reid, C. Dupraz, A. W. Decho, D. H. Buckley, J. R. Spear, K. M. Przekop, and P. T. Visscher.** 2006. Sulfate reducing bacteria in microbial mats: changing paradigms, new discoveries. Sediment. Geol. **185:** 131–145.
6. **Bissett, A., D. De Beer, R. Schoon, F. Shaaishi, A. Reimer, and G. Arp.** 2008. Microbial mediation of tufa formation in karst-water creeks. Limnol. Oceanogr. **53:**1159–1168.
7. **Broeker, W. S., and T. H. Peng.** 1974. Gas exchange rates between air and sea. Tellus B **26:**21–35.
8. **Burne, R. V., and L. S. Moore.** 1987. Microbialites: organosedimentary deposits of benthic microbial communities. Palaios **2:**241–254.
9. **de Beer, D., M. Kühl, N. Stambler, and L. Vaki.** 2000. A microsensor study of light enhanced Ca^{2+} uptake and photosynthesis in the reef-building hermatypic coral Favia sp. Mar. Ecol. Prog. Ser. **194:**175–185.
10. **de Beer, D., A. Schramm, C. M. Santegoeds, and M. Kühl.** 1997. A nitrite microsensor for profiling environmental biofilms. Appl. Environ. Microbiol. **63:**973–977.
11. **Dittrich, M., B. Müller, D. Mavrocordatos, and B. Wehrli.** 2003. Induced calcite precipitation by cyanobacterium *Synechococcus*. Acta Hydrochim. Hydrobiol. **31:**162–169.
12. **Drysdale, R., S. Lucas, and K. Carthew.** 2003. The influence of diurnal temperatures on the hydrochemistry of a tufa-depositing stream. Hydrol. Process. **17:**3421–3441.
13. **Grotzinger, J. P., and J. F. Kasting.** 1993. New constraints on Precambrian ocean composition. J. Geol. **101:**235–243.
14. **Kempe, S., and J. Kazmierczak.** 1990. Calcium carbonate supersaturation and the formation of in situ calcified stromatolites, p. 255–278. *In* V. Ittekot, S. Kempe, W. Michaelis, and A. Spitzy (ed.), Facets of modern biogeochemistry. Springer, Berlin, Germany.
15. **Larkum, A. W. D., E. C. Koch, and M. Kühl.** 2003. Diffusive boundary layers and photosynthesis of the epilithic algal community of coral reefs. Mar. Biol. **142:**1073–1082.
16. **Li, Y., and S. Gregory.** 1974. Diffusion of ions in seawater and in deep-sea sediments. Geochim. Cosmochim. Acta **38:**703–714.
17. **McConnaughey, T. A., and J. F. Whelan.** 1997. Calcification generates protons for nutrient and bicarbonate uptake. Earth Sci. Rev. **42:**95–117.
18. **Merz, M. U. E.** 1992. The biology of carbonate precipitation by cyanobacteria. Facies **26:**81–102.
19. **Pentecost, A.** 1985. Association of cyanobacteria with tufa deposits: identity, enumeration and nature of the sheath material revealed by histochemistry. Geomicrobiol. J. **4:**285–298.
20. **Plummer, L. N., and E. Busenberg.** 1982. The solubilities of calcite, aragonite and vaterite in CO_2-H_2O solutions between 0 and 90°C, and an evolution of aqueous model for the system $CaCO_3$-CO_2-H_2O. Geochim. Cosmochim. Acta **46:**1011–1040.
21. **Reid, R. P., P. T. Visscher, A. W. Decho, J. F. Stolz, B. M. Bebout, C. Dupraz, I. G. Macintyre, H. W. Paerl, J. L. Pinckney, L. Prufert-Bebout, T. F. Steppe, and D. J. DesMarais.** 2000. The role of microbes in accretion, lamination and early lithification of modern marine stromatolites. Nature **406:**989–992.
22. **Reitner, J.** 1993. Modern cryptic microbialite/metazoan facies from Lizard Island (Great Barrier Reef, Australia). Formation and concepts. Facies **29:**3–40.
23. **Revsbech, N. P.** 1989. An oxygen microsensor with a guard cathode. Limnol. Oceanogr. **34:**474–478.
24. **Riding, R.** 1991. Calcified cyanobacteria, p. 55–87. *In* R. Riding (ed.), Calcareous algae and stromatolites. Springer, Berlin, Germany.
25. **Riding, R.** 2000. Microbial carbonates: the geological record of calcified bacterial-algal mats and biofilms. Sedimentology **47:**179–214.
26. **Riding, R.** 1992. Temporal variation in calcification in marine cyanobacteria. J. Geol. Soc. London **149:**979–989.
27. **Riding, R.** 1999. The term stromatolite: towards an essential definition. Lethaia **32:**321–330.
28. **Riding, R., and L. Liang.** 2005. Geobiology of microbial carbonates: metazoan and seawater saturation state influences on secular trends during the Phanerozoic. Palaeogeogr. Palaeoclimatol. Palaeoecol. **219:**101–115.
29. **Shiraishi, F., A. Bissett, D. de Beer, A. Reimer, and G. Arp.** 2008. Photosynthesis, respiration and exopolymer calcium-binding in biofilm calcification (Westerhöfer and Deinschwanger Creek, Germany). Geomicrobiol. J. **25:** 83–94.
30. **Soetaert, K., A. F. Hofmann, J. J. Middleburg, F. J. R. Meysman, and J. Greenwood.** 2007. The effect of biogeochemical processes on pH. Mar. Chem. **105:**30–51.
31. **Thompson, J. B., and F. G. Ferris.** 1990. Cyanobacterial precipitation of gypsum, calcite, and magnesite from natural alkaline lake water. Geology **18:**995–998.
32. **Trichet, J., and C. Defarge.** 1995. Non-biologically supported organomineralization. Bull. Inst. Oceanogr. **14:**203–236.
33. **Walter, M. R., and G. R. Heys.** 1985. Links between the rise of the metazoa and the decline of stromatolites. Precambrian Res. **29:**149–174.
34. **Wray, J. L.** 1977. Calcareous algae (developments in palaeontology and stratigraphy), vol. 4. Elsevier, Amsterdam, The Netherlands.